Organic Electronics 33 (2016) 78–87

Contents lists available at ScienceDirect

Organic Electronics

journal homepage: www.elsevier.com/locate/orgel

The synthesis, crystal structures, aggregation-induced emission and electroluminescence properties of two novel green-yellow emitters based on carbazole-substituted diphenylethene and dimesitylboron

Heping Shi [a, *, 1], Dehua Xin [a, 1], Sheng-Di Bai [a], Li Fang [a], Xin-E Duan [a], Jesse Roose [b], Huiren Peng [c], Shuming Chen [c, **], Ben Zhong Tang [b, d, ***]

[a] School of Chemistry and Chemical Engineering, Shanxi University, Taiyuan 030006, PR China
[b] Department of Chemistry, Institute for Advanced Study, Division of Biomedical Engineering, Division of Life Science, State Key Laboratory of Molecular Neuroscience, Institute of Molecular Functional Materials, The Hong Kong University of Science and Technology, Clear Water Bay, Kowloon, Hong Kong, China
[c] Department of Electrical and Electronic Engineering, South University of Science and Technology of China, Shenzhen, Guangdong 518055, PR China
[d] State Key Laboratory of Luminescent Materials and Devices, South China University of Technology, Guangzhou, Guangdong 510640, PR China

ARTICLE INFO

Article history:
Received 23 January 2016
Received in revised form
1 March 2016
Accepted 4 March 2016
Available online 16 March 2016

Keywords:
Diphenylethene
Carbazole
Dimesitylboron
Aggregation-induced emission
Electroluminescence

ABSTRACT

Introducing the hole-transporting carbazole moiety into an aggregation-induced emissive tetraarylethene skeleton and attaching electron-transporting dimesitylboron groups to the periphery, we obtain two novel electroluminescent materials. Their structures are fully characterized by elemental analysis, mass spectrometry, NMR spectroscopy and X-ray crystallography. Furthermore, their thermal, electrochemical, as well as photophysical properties including AIE-behavior are systematically investigated not only by experimental methods but also by DFT computation. Thereby, we show that the two compounds possess high thermal and electrochemical stability with a remarkable AIE-behavior. X-ray crystal analyses aided by DFT calculations provide insights in the origin of the luminescent properties and AIE features. Ultimately, two non-doped OLEDs (Device A and Device B) were fabricated by using **PDPBCE** and **BDPBCE** as light-emitting layer, respectively. Device A showed yellowish-green light with a turn-on voltage of 3.8 V, a maximum brightness of 59130 cd m^{-2} and a maximum current efficiency of 6.43 cd A^{-1}. Device B exhibited greenish-yellow light with a turn-on voltage of 3.0 V, a maximum brightness of 67,500 cd m^{-2} and a maximum current efficiency of 11.2 cd A^{-1}.

1. Introduction

Development of organic light-emitting diodes (OLEDs) has been a hot topic of current research because of their applications in displays and lighting [1]. In OLEDs, the light-emitting materials are commonly fabricated as thin films, whose quality plays a key role in the eventual performance of the device. To date, scientists have synthesized a variety of luminescent materials [2–8]. Unfortunately, most fluorescent molecules with conventional π-conjugated planar chromophores suffer from the aggregation-caused quenching (ACQ) effect [9], namely, they have very high luminescence efficiency in solutions, but show relatively weak or no emissions in solid state. Such aggregation-caused fluorescence quenching is attributed to the formation of delocalized excitons via strong intermolecular π–π interactions and radiationless decay [10–14]. Due to the ACQ effect, most fluorophores cannot be utilized in high performance devices, whereas those ACQ fluorophores suitable require additional measures such as doping to counter the negative effects [15,16]. Therefore, the development of high-performance light-emitting materials without ACQ effect remains a challenge to researchers.

To overcome the ACQ effect, Tang and co-workers were the first

* Corresponding author.
** Corresponding author.
*** Corresponding author. Department of Chemistry, Institute for Advanced Study, Division of Biomedical Engineering, Division of Life Science, State Key Laboratory of Molecular Neuroscience, Institute of Molecular Functional Materials, The Hong Kong University of Science and Technology, Clear Water Bay, Kowloon, Hong Kong, China.
E-mail addresses: hepingshi@sxu.edu.cn (H. Shi), chen.sm@sustc.edu.cn (S. Chen), tangbenz@ust.hk, msqinaj@scut.edu.cn (B.Z. Tang).
[1] Heping Shi and Dehua Xin contributed equally to this work.

http://dx.doi.org/10.1016/j.orgel.2016.03.003
1566-1199/

ones to report on the aggregation-induced emission (AIE) effect in 2001 [17]. AIE is an unusual phenomenon relating to molecules – often propeller shaped – that are not luminescent in solution, but become highly emissive in aggregated state. In their successive studies, the restriction of intramolecular motion (RIM), including the restriction of intramolecular rotation (RIR), and the restriction of intramolecular vibration (RIV), in the aggregated state were proposed as the principal reason for AIE phenomenon. Many research groups have recognized and provided further evidence for the RIM being the working mechanism to explain this phenomenon [18–22]. So far, a vast number of AIE-active fluorescent materials have been reported [23–31]. Among the reported AIE fluorescent materials, tetraphenylethene (TPE) is most widely used as a building block to construct AIE-active molecules owning to its facile synthesis that tolerates many different functional groups and its excellent AIE effect [32–39].

Carbazole-derivatives mostly functionalized at the 2,7-, 3,6- or the 9-position have been frequently exploited as luminescent materials in OLEDs due to their comparatively high HOMO energy levels and outstanding hole-transporting capabilities [40–42]. However, carbazole and most of its derivatives suffer from the ACQ effect [43,44]. Owing to the unique AIE effect of TPE and excellent hole-transporting property of carbazole, an effective synthetic strategy to construct efficient luminescent materials with both good charge-transporting properties and efficient solid-state emission is established by fusing carbazole and TPE units together. For example, Tang et al. synthesized a carbazole-containing tetraphenylethene by incorporation two 3-carbazolyl groups to the 1,2-position of diphenylethylene, exhibiting an electroluminescence performance with maximum current efficiency, maximum luminance and external quantum efficiency up to 5.7 cd A^{-1}, 5060 cd m^{-2} and 2.3%, much higher than that of TPE (0.45 cd A^{-1}, 1800 cd m^{-2} and 0.4%) [45]. The amazing result is based on the good hole-transport ability of carbazole groups.

The dimesitylboron group has been commonly used in molecules for light-emitting devices due to its strong electron-donating ability [46–49], originating from the p_π-π^* conjugation between the vacant p-orbital on the boron atom with the π^* orbital of the conjugated framework [50]. In addition, the bulky dimesityl groups can suppress the π–π stacking, which favors the solid-state emission. Thus, the introduction of the dimesitylboron group into the TPE structure facilitates the electron-transport capability of the highly fluorescent solid emitters. For example, Tang et al. synthesized an emitter through combination of AIE-active units (TPE) and the dimesitylboron group [51]. This molecule had been proven to be a promising bifunctional material in the fabrication of a non-doped OLED device. The maximum current efficiency, maximum luminance and external quantum efficiency of the corresponding OLED was be high as 5.78 cd A^{-1}, 5581 cd m^{-2} and 2.3%. It is certain that the incorporation of inherently electron deficient dimesitylboron group is beneficial to enhance the electron-transporting ability. Based on previous research results, we became interested fusing tetraphenylethene, carbazole, and dimesitylboron groups together into a single molecule to obtain novel materials with excellent luminescent, hole-transporting and electron-transporting properties. It is envisioned that the electroluminescent performance using these novel materials in an OLED as the light-emitting layers can be greatly improved.

In this paper, we successfully synthesized two novel compounds, 3,3′-{1-[4-(dimesitylboryl)phenyl]-2-phenylethene-1,2-diyl}*bis*(9-ethyl-9*H*-carbazole) (**PDPBCE**) and 1,2-*bis*[4-(dimesitylboryl)phenyl]-1,2-*bis*(9-ethyl-9*H*-carbazol-3-yl)ethene (**BDPBCE**), both comprised a carbazole-substituted diphenylethene and dimesitylboron groups. The thermal, electrochemical and photophysical properties, the crystal structures and the quantum chemistry calculations of the two compounds were studied to reveal the luminescent properties and molecular structure-property correlations. Furthermore, the electroluminescence properties of the two compounds were investigated by using the compounds as light-emitting layer in non-doped OLEDs. The results showed that both the devices exhibited efficient performances with low turn-on voltages, high brightnesses and high current efficiencies, demonstrating that **PDPBCE** and **BDPBCE** are potential candidates for fabricating luminescent devices.

2. Experimental section

2.1. Materials and instruments

All reagents were used as received from commercial sources without further purification unless otherwise stated. Solvents were freshly distilled according to the standard procedures. Tetrahydrofuran (THF) was distilled from sodium benzophenone ketyl under dry nitrogen immediately prior to use.

2.1.1. Synthesis of (4-bromophenyl)(9-ethyl-9H-carbazol-3-yl) methanone (1)

A stirred mixture of *N*-ethylcarbazole (1.953 g, 10 mmol) and of 4-bromobenzoylchloride (1.410 g, 10 mmol) in 35 mL CH_2Cl_2 was slowly treated with aluminum chloride (1.330 g, 10 mmol) under nitrogen. The mixture was heated at 40 °C for 24 h. After cooling to room temperature, cold water (200 mL) was added to the residue. The organic layer was extracted with dichloromethane (3 × 50 mL), washed with water and diluted hydrochloric acid. The crude product was purified by silica-gel chromatography to give a white solid in 70% yield (2.65 g). ^{1}H NMR (600 MHz, $CDCl_3$) δ (ppm): 8.57 (d, J = 1.86 Hz, 1H), 8.12–8.11 (d, J = 7.81 Hz, 1H), 8.01–7.99 (d, J = 6.77 Hz, 1H), 7.72 (s, 1H), 7.71 (s, 1H), 7.66 (s, 1H), 7.65 (s, 1H), 7.53 (t, J = 14.14 Hz, 1H), 7.47–7.45 (t, J = 15.01 Hz, 2H), 7.31–7.28 (t, J = 13.63 Hz, 1H), 4.44–4.40 (q, J = 21.15 Hz, 2H), 1.49–1.47 (t, J = 14.36 Hz, 3H).

Synthesis of 1,2-*bis*(4-bromophenyl)-1,2-*bis*(9-ethyl-9*H*-carbazol-3-yl)ethene (2).

A 250 mL flask equipped with a stirrer was loaded with zinc powder (4.628 g, 71.2 mmol) and 150 mL THF. $TiCl_4$ (4.00 mL, 40 mmol) was slowly added by a syringe at −78 °C under nitrogen. The mixture was allowed to warm to room temperature and then heated to reflux for 4 h. After cooling to room temperature, **1** (3.42 g, 9.0 mmol) in 40 mL THF solution was added to the mixture, which subsequently was heated at 70 °C overnight. Then, the reaction was quenched with 10% K_2CO_3 aqueous solution and extracted with dichloromethane (3 × 50 mL). The organic layer was collected and concentrated in vacuo. The crude product was purified by silica-gel chromatography to give a yellow-green solid (2.4 g, 75%). ^{1}H NMR (600 MHz, $CDCl_3$) δ (ppm): 7.90–7.80 (q, 2H), 7.75–7.72 (t, 2H), 7.45–7.30 (m, 4H), 7.28–7.24 (m, 3H), 7.32 (d, 1H), 7.18–7.08 (m, 6H), 7.07–6.97 (m, 5H), 4.34–4.20 (m, 4H), 1.45–1.32 (m, 6H).

Synthesis of 3,3′-{1-[4-(dimesitylboryl)phenyl]-2-phenylethene-1,2-diyl}*bis*(9-ethyl-9*H*-carbazole) (**PDPBCE**) and 1,2-*bis*[4-(dimesitylboryl)phenyl]-1,2-*bis*(9-ethyl-9*H*-carbazol-3-yl)ethene (**BDPBCE**).

A 100 mL round-bottom flask with **2** (1.450 g, 2.0 mmol) was evacuated under a vacuum and flushed with dry nitrogen three times. Then, dry THF (80 mL) was added. The mixture was cooled to −78 °C, *t*-BuLi (4.60 mL, 1.3 M in hexane, 6.00 mmol) was added dropwise by a syringe, and stirring continued for 4 h at −78 °C. Subsequently, dimesitylboron fluoride (2.144 g, 8.0 mmol) was slowly added to the reaction solution. The mixture was warmed slowly to room temperature and stirred for 24 h. Then, the mixture

was quenched with ice water (200 mL) and stirred for 2 h. The organic layer was extracted with dichloromethane (3 × 50 mL) and the combined organic extracts were dried over anhydrous $MgSO_4$. After filtration and solvent evaporation, the crude product was firstly purified by silica gel column chromatography. At last, **PDPDCE** and **BDPBCE** were separated by recycling chromatography.

PDPBCE was obtained as a green solid in 25% yield (0.40 g). IR (KBr), υ/cm^{-1}: 3052, 2971, 2924, 2849, 1596, 1464, 1385, 1334, 1231, 1124, 1010, 845, 813, 747. ^{1}H NMR (600 MHz, $CDCl_3$) δ (ppm): 7.84–7.76 (m, 4H), 7.41–7.30 (m, 4H), 7.26–7.00 (m, 14H), 6.78–6.66 (m, 4H), 4.33–4.21 (m, 4H), 2.28–2.20 (m, 6H), 2.01–1.80 (m, 12H), 1.43–1.32 (m, 6H). ^{13}C NMR (600 MHz, $CDCl_3$) δ (ppm): 152.23, 147.83, 147.61, 144.62, 144.48, 143.74, 143.69, 143.13, 141.64, 141.25, 138.72, 138.66, 137.59, 134.67, 134.23, 132.84, 132.61, 130.50, 128.30, 126.01, 125.44, 123.35, 123.15, 121.62, 121.52, 111.33, 110.45, 110.27, 40.41, 26.27, 24.06, 24.00, 16.73, 16.64, 3.90, 2.88. MS: (*m/z*) 814.4. Anal. Calcd for $C_{60}H_{55}BN_2$: C 88.43%, H 6.80%, B 1.33% and N 3.44%. Found: C 88.60%, H 6.85%, and N 3.50%.

BDPBCE was obtained as a yellow solid in 20% yield (0.41 g). IR (KBr), υ/cm^{-1}: 3047, 3015, 2990, 2920, 2849, 1620, 1605, 1486, 1358, 1231, 1153, 1023, 846, 801, 718, 668. ^{1}H NMR (600 MHz, $CDCl_3$) δ (ppm): 7.80–7.75 (m, 4H), 7.42–7.34 (m, 3H), 7.32–7.29 (d, 1H), 7.22–7.17 (m, 5H), 7.16–7.06 (m, 8H), 7.04–7.01 (m, 1H), 6.81–6.66 (m, 8H), 4.34–4.20 (m, 4H) 2.28–2.20 (m, 12H) 1.99–1.96 (m, 24H), 1.46–1.32 (m, 6H). ^{13}C NMR (600 MHz, $CDCl_3$) δ (ppm): 151.93, 147.26, 146.7, 144.78, 143.68, 143.14, 141.72, 141.66, 141.27, 138.73, 137.46, 134.32, 132.73, 132.50, 130.99, 128.33, 126.73, 126.44, 125.99, 125.41, 123.21, 121.61, 111.28, 110.48, 110.33, 63.23, 40.46, 32.58, 26.28, 24.08, 24.00, 17.09, 16.73, 16.63, 3.90, 2.87. MS: (*m/z*) 1062.6. Anal. Calcd for $C_{78}H_{76}B_2N_2$: C 88.13%, H 7.20%, B 2.03 and N 2.64%. Found: C 88.23%, H 7.21%, and N 2.67%.

2.2. Measurements and characterization

All NMR spectra were measured on a Bruker 600 MHz spectrometer. Thermogravimetric analysis (TGA) was performed on a TGA 2050 thermogravimetric analyzer under an N_2 atmosphere with a heating rate of 10 °C/min from room temperature to 750 °C. Differential scanning calorimetry (DSC) was performed using a Q2000 DSC differential scanning calorimeter under a N_2 atmosphere with a heating rate of 10 °C/min from room temperature to 250 °C. Elemental analyses were performed on an Element Analysis System. Mass spectra were recorded with an LC-MS system consisting of a Waters 1525 pump and a Micromass ZQ4000 single quadrupole mass spectrometer detector. Cyclic voltammetry (CV) was performed on a CHI-600C electrochemical analyzer. The CV measurements were carried out with a conventional three-electrode configuration consisting of a glassy carbon working electrode, a platinum-disk auxiliary electrode and an Ag/AgCl reference electrode, and the scan speed was 50 mV s^{-1}. UV–vis absorption spectra were acquired on a Shimadzu UV-2450 absorption spectrophotometer. Fluorescence spectra were obtained on a Hitachi F-4500 spectrofluorometer. The fluorescence quantum yield was determined using quinine sulfate as the reference (excited at 350 nm). All measurements were performed at room temperature.

2.3. Single crystal X-ray diffraction

The single crystals of **PDPBCE** and **BDPBCE** were obtained by the slow diffusion of their respective **$CHCl_3$: methanol (2:1, v/v)** layered solutions over the period of several days at room temperature. Since the two crystals are stable under ambient conditions, the data collection was performed without any insert gas protection at room temperature on a Bruker SMART APEX-II CCD area detector using graphite-monochromated Mo Kα radiation (λ = 0.71073 Å). Data reduction and integration, together with global unit cell refinements were conducted by the INTEGRATE program of the APEX2 software. Semi-empirical absorption corrections were applied using the SCALE program for area detector. The structures were solved by direct methods and refined by the full matrix least-squares methods on F [2] using SHELX.

2.4. Device fabrication and measurement

The multilayer OLEDs were fabricated by a vacuum-deposition method. Organic layers were fabricated by high-vacuum (5×10^{-4} Pa) thermal evaporation onto a glass (3 cm × 3 cm) substrate precoated with an ITO layer. Dipyrazinoquinoxaline-2,3,6,7,10,11-hexacarbonitrile (HATCN) was used as the hole injection layer, *N*,*N*-bis(naphthalene)-*N*,*N*-*bis*(phenyl)benzidine (NPB) was used as the hole-transport layer (HTL), **PDPBCE** and **BDPBCE** were used as the emitting layer, 1,3,5-tri(1-phenyl-1*H*-benzo[*d*] imidazol-2-yl)phenyl (TPBi) was used as the electron-transport layer (ETL) and LiF/Al was evaporated as the cathode. All organic layers were sequentially deposited. Thermal deposition rates for organic materials, LiF and Al were 0.5 Å/s, 0.5 Å/s and 1 Å/s, respectively. The active area of the devices is 9.0 mm^2. The EL spectra were measured on a Hitachi MPF-4 fluorescence spectrometer. The voltage current density characteristics of OLEDs were recorded on a Keithley 2400 Source Meter. The characterization of brightness current-voltage was measured with a 3645 DC power supply combined with a 1980A spot photometer and were recorded simultaneously. All measurements were done at room temperature.

3. Results and discussion

3.1. Synthesis and characterization

PDPBCE and **BDPBCE** were obtained following the synthetic routes shown in Scheme 1. Firstly, compound **1** was synthesized by reacting 4-bromobenzoyl chloride with *N*-ethylcarbazole in a Friedel-Crafts-Acylation. A subsequent McMurry coupling under standard conditions using $TiCl_4$ as a titanium source gave the dibrominated intermediate **2**. The target compounds, **PDPBCE and BDPBCE**, were synthesized by reacting compound **2** with *n*-BuLi, followed by the addition of dimesitylboron fluoride at −78 °C. Due to the similar molecular structure and crystallizability, **PDPBCE and BDPBCE** cannot be separated by silica gel column chromatography and recrystallization. They were separated by using recycling chromatography. All the intermediate structures were confirmed by ^{1}H NMR, whereas the final products were fully characterized by ^{1}H NMR, ^{13}C NMR, MS and X-ray diffraction. **PDPBCE** and **BDPBCE** show good solubility in common organic solvents, such as toluene, dichloromethane, chloroform and tetrahydrofuran, but are insoluble in water.

3.2. Thermal properties

Generally, the thermal stability of a luminogen qualitatively reflects its average life-time in a device. The thermal properties of **PDPBCE** and **BDPBCE** were investigated by thermogravimetric analysis (TGA) and differential scanning calorimetry analysis (DSC). As evidenced by the data depicted in Fig. S1 (SI), both **PDPBCE** and **BDPBCE** showed excellent thermal stability, losing 5% of their weight at decomposition temperatures (T_d) as high as 228 and 235 °C, respectively, presumably due to the sterically shielding effect of the carbazole and dimesitylboron groups. **BDPBCE** possessed a higher decomposition temperature than the **PDPBCE**,

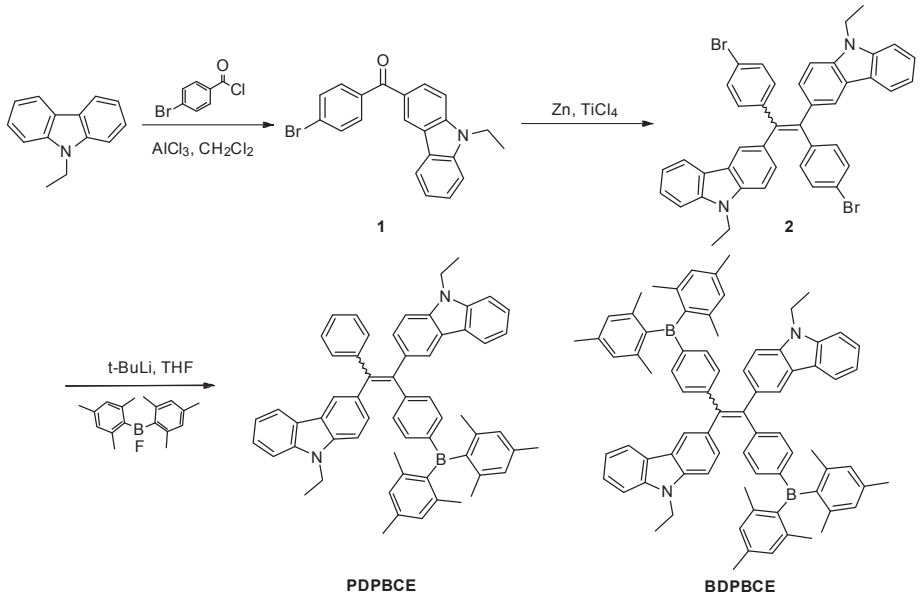

Scheme 1. Synthetic route of **PDPBCE** and **BDPBCE**.

which is due to the larger molecular weight. The DSC curves of the two compounds are shown in Fig. S2. Glass transition temperatures (T_g) for **PDPBCE** and **BDPBCE** were found to be 95 and 139 °C, respectively. Having both a high T_d and T_g are promising features for a material to fabricate efficient EL devices.

3.3. Photophysical properties

The UV–Vis absorption and fluorescence spectra of **PDPBCE** and **BDPBCE** in different solutions of different polarity (10 μM) are shown in Fig. S3 with the key data being listed in Table 1. As illustrated in Fig. S3, the absorption features of **PDPBCE** and **BDPBCE** were similar to each other due to their homologous molecular skeleton, they all exhibited a sharp absorption band at 305 nm and a broad absorption band centered at 400 nm. The sharp band could be associated with the π–π* transition of the molecular skeleton, while the long-wavelength absorption originated from the intramolecular charge transfer (ICT) from the electron-donating carbazole moieties to the electron-withdrawing dimesitylboron groups. The absorption spectra of **PDPBCE** and **BDPBCE** showed analogous maxima in the different solvents, inferring that their structure and electronic characteristics of the ground state are independent of the solvent polarity. The optical energy band gaps (E_g^{opt}) estimated from the onset wavelengths of the UV absorptions were calculated to amount to 3.02 eV and 2.95 eV for **PDPBCE** and **BDPBCE**, respectively.

The photoluminescence (PL) spectra of **PDPBCE** and **BDPBCE** in different solvents displayed interesting features because of the twisted geometry conformation and the complicated electronic effect. As shown in Fig. S4, **PDPBCE** and **BDPBCE** showed poor emission in dilute solutions, presumably as a result of intramolecular rotations that lead to non-radiative decay. It was observed that the fluorescence of both **PDPBCE** and **BDPBCE** were dependent on the solvent. In non-polar hexane, **PDPBCE** exhibited a strong emission peak at 356 nm and 372 nm, a weak emission peak at 443 nm, which is assigned to the locally excited state (LE) emission and the twisted intramolecular charge transfer (TICT) emission. It is worth to note that there only a slight emission band centered at 520 nm was observed, which could be associated with the intramolecular charge transfer (ICT). In hexane, **BDPBCE** exhibited three emission peaks with maxima at 392 nm, 450 nm, and 550 nm, which were assigned to the LE, TICT, and CT, respectively. With increasing of solvent polarity, LE emission remains unchanged, while there is a significantly bathochromic shift taking place for the TICT and CT emission.

Since the solid state emission is essential for applying luminescent materials in OLED devices, we examined the PL spectra of the **PDPBCE** and **BDPBCE** as thin films, shown in Fig. S5. Unlike the

Table 1
Physical property of **PDPBCE** and **BDPBCE**.

Com.	λ_{abs}[a] (nm)	λ_{em}[b] (nm)	λ_{em}[c] (nm)	Φ[d]	T_d[e] (°C)	T_g[e] (°C)	HOMO/LUMO[f] (eV)	E_g[g] (eV)	HOMO/LUMO[h] (eV)	E_g[h] (eV)
PDPBCE	305 395	530	520	0.68	228	95	−4.78/−1.46	3.02	−4.82/−1.61	3.21
BDPBCE	305 408	553	540	0.70	235	139	−4.85/−1.90	2.95	−4.87/−1.77	3.10

[a] Measured in THF.
[b] Measured in THF + H_2O(1:9).
[c] Measured in film.
[d] Measured in THF + H_2O(5:95).
[e] Obtained from TGA and DSC.
[f] Obtained from CV in CH_3CN/n-Bu_4NClO_4 and estimated from HOMO = −(4.4 + E^{ox}_{onset}); LUMO = HOMO + E_g.
[g] Calculated from the absorption edge, $E_g = 1240/\lambda_{onset}$.
[h] Obtained from DFT calculation.

emission in solutions, the two compounds exhibited strong green emission with a maximum peaks at 520 nm and 540 nm. The spectra of **BDPBCE** were 20 nm red-shifted compared to **PDPBCE**, possibly due to the larger molecular conjugation in addition to the stronger intermolecular interactions between the molecules. The bright green solid state emitting performances make both compounds possible candidates for green OLED devices.

As before-mentioned, due to the fact that both **PDPBCE** and **BDPBCE** were comprised of a tetraarylethene core, AIE-behavior was observed. In order to investigate the AIE-properties more carefully, their PL emissions were recorded in THF/water mixtures with different volume fractions of water, while the concentration was kept at 2 μM. Fig. 1 (a) depicts the PL spectra of **PDPBCE** and **BDPBCE** in THF and THF/water mixtures at an excitation wavelength of 330 and 350 nm, respectively. **PDBDCE** exhibits two main emission bands in pure THF, the peaks with maxima at 373 nm and 442 nm were corresponding to the LE and TICT emissions, respectively. As the water fraction increased from 0% to 95%, the TICT emission resulted in a red-shift from 442 to 468 nm and a decrease of the PL intensity. Starting at a water content of 70%, a new green emission band centered at 540 nm appeared, suggesting this band being caused by the aggregation of the molecules. Higher water contents increased the number and size of aggregates, thereby enhancing its light emission to a greater extent until a maximum was reached for a water content of 95%. Furthermore, the emission was blue-shifted to 530 nm, which can be explained by the less polar environment inside the nanoparticles attenuating the CT effect. **BDPBCE** exhibited broad emission bands with two maximum peaks at 383 and 423 nm, which could be associated with the LE and TICT emission, whose emission intensity was weak as a function of water content. Similarly to **PDPBCE**, a new emission band at 553 nm was observed with water fractions higher than 70%, whose intensity increased to its maximum at a water fraction of 95%. As shown by the AIE-curves in Fig. 1(b), the PL intensities of **PDPBCE** and **BDPBCE** in the 95% aqueous solutions were 169 and 191-fold higher compared to those in pure THF. The fluorescence quantum yields (Φ) of **PDPBCE** and **BDPBCE** in 95% aqueous solutions were found to be 0.68 and 0.70, respectively. Fig. 1(c) illustrates the photographic images of **PDPBCE** and **BDPBCE** in THF/water mixtures of f_w (i) 0.0 and (ii) 95%, visualizing the remarkable AIE properties. This typical AIE effect was attributed to the RIR of the tetraarylethene skeleton, which leads to blocking of the non-radiative decay pathway thus enhancing the emission.

3.4. X-ray studies and AIE mechanism

Study of the X-ray single-crystal structures as an efficient tool for acquiring the molecular structure to reveal the molecular structure-property correlations, single crystals of **PDPBCE** and **BDPBCE** were obtained by slow diffusion of a $CHCl_3$-MeOH solvent system. Their individual ORTEP structures and crystal packing motifs are shown in Figs. 2 and 3. The single crystal study reveals that the crystal of **PDPBCE** belongs to triclinic space group P-1 with $Z = 2$, while the crystal structure of **BDPBCE** belongs to the monoclinic space group C2/c with $Z = 4$. The intramolecular torsion angels of the aromatic rings in **PDPBCE** and **BDPDCE** (Table 2) ranged between 48.5° and 85.2°, confirming the strongly twisted conformation of the two compounds. For instance, in crystal of **PDPBCE**, the torsion angles between phenyl ring Cg(7) and carbazole ring Cg(5), phenyl ring Cg(6), and carbazole ring Cg(5) were 82.60°, 48.57°, and 70.48°, respectively. In the crystal of **BDPBCE**, the dihedral angels between phenyl ring Cg(3) and carbazole ring Cg(5), phenyl ring Cg(3′) and carbazole ring Cg(5′) amounted to 73.20°, 61.61°, and 66.16°, respectively. As revealed by the single X-ray crystal structures, displayed in Fig. 2, all aryl substituents in both compounds adopted a twisted conformation with regard to the olefinic double bond, resulting in a propeller-like arrangement. These twisted conformations contribute to the AIE effect. The twisted conformations support active intramolecular rotations in solution leading to poor fluorescence, while preventing the molecules form π−π stacking in the solid phase due to the non-planar conformations, which has been further investigated with the PLATON calculations. Both effects resulted in the AIE feature of the compounds. Calculated by PLATON, we found that the distances between all the aromatic rings of **PDPBCE** and **BDPBCE** ranged between 4.02 and 5.98 Å, which means there are no classical π-π interactions can be observed in neither crystals [52]. The crystal packing (Fig. 3), revealed that the dominant intramolecular interactions of **PDPBCE** (Fig. 3(a)) consisted of C—H ··· π hydrogen bonds. For instance, The hydrogen bonds of C(53)—H(53B) ··· Cg(8), C(50)—H(50A) ··· Cg(9) with distance of 3.396 Å and 2.684 Å are formed between the methyl protons in the dimesitylboron units of one molecule and the phenyl rings in dimesitylboron units of the neighboring molecules. The hydrogen bonds of C(13)—H(13) ··· Cg(5), C(21)—H(21) ··· Cg(4), and C(60)—H(60) ··· Cg(3) with distances of 3.752 Å, 3.062 Å, and 3.628 Å were formed between the carbazolyl protons and the phenyl rings of carbazolyl groups of the adjacent molecules. In the packing diagram of **BDPBCE** in Fig. 3(b), one **BDPBCE** molecule and its three adjacent molecules formed five different kinds of C—H ··· π bonds. For example, The hydrogen bond of C(41)—H(41) ··· Cg(4) having a distance of 3.135 Å was formed between the carbazolyl protons of one molecule and the phenyl rings in the dimesitylboron units of the neighboring molecules. The hydrogen bonds of C(34)—H(34A) ··· Cg(1′) and C(35)—H(35B) ··· Cg(6′) with distances of 3.099 Å and 3.199 Å were formed between the methyl protons in the dimesitylboron units of one molecule and the phenyl rings in carbazolyl units of the neighboring molecules. All the distances of the hydrogen bonds in **PDPBCE** and **BDPBCE** are listed in Table 2. As discussed above, multiple hydrogen bonds were formed between the aromatic rings and the protons of the neighboring molecules in **PDPBCE** and **BDPBCE**. Such intermolecular interactions could assist in locking the molecular motion in the crystal lattice and reducing the non-radiative deactivation of excitons, which contributes to the AIE effect for the two compounds [53].

3.5. Theoretical calculation

To further investigate the photophysical property and the structure-property relationship of **PDPBCE** and **BDPBCE**, the optimized molecular structures and spatial distributions of HOMOs and LUMOs were calculated by density function theory (DFT) at the B3LYP/6-31g* level using the Gaussian 09 package. Fig. 4 shows the optimized geometries and the orbital distributions of HOMO and LUMO energy levels of **PDPBCE** and **BDPBCE**. The optimized molecular structures showed similar conformations with the X-ray studies, which disclosed that both **PDPBCE** and **BDPBCE** adopt a quite non-planar twisted conformation with the four substituted aromatic rings constructed from a propeller-like shape along the olefinic double-bond. The electron distributions of the HOMO level of **PDPBCE** is mainly located at the electron rich carbazole units and the ethene core, whereas the LUMO is mainly located at the dimesitylboron group and the olefinic double-bond. Similarly, for **BDPBCE** the HOMO is mainly located on the olefin and carbazole units and the LUMO electron distributions predominantly locate on the ethene core and dimesitylboron units. Such orbital distributions reveal an intrinsic intramolecular charge transfer (ICT) from the carbazole (electron-donor) to the dimesitylboron (electron-acceptor) moiety. **BDPBCE** showed similar orbital distributions in comparison with **PDPBCE**. The calculated band gaps for **PDPBCE**

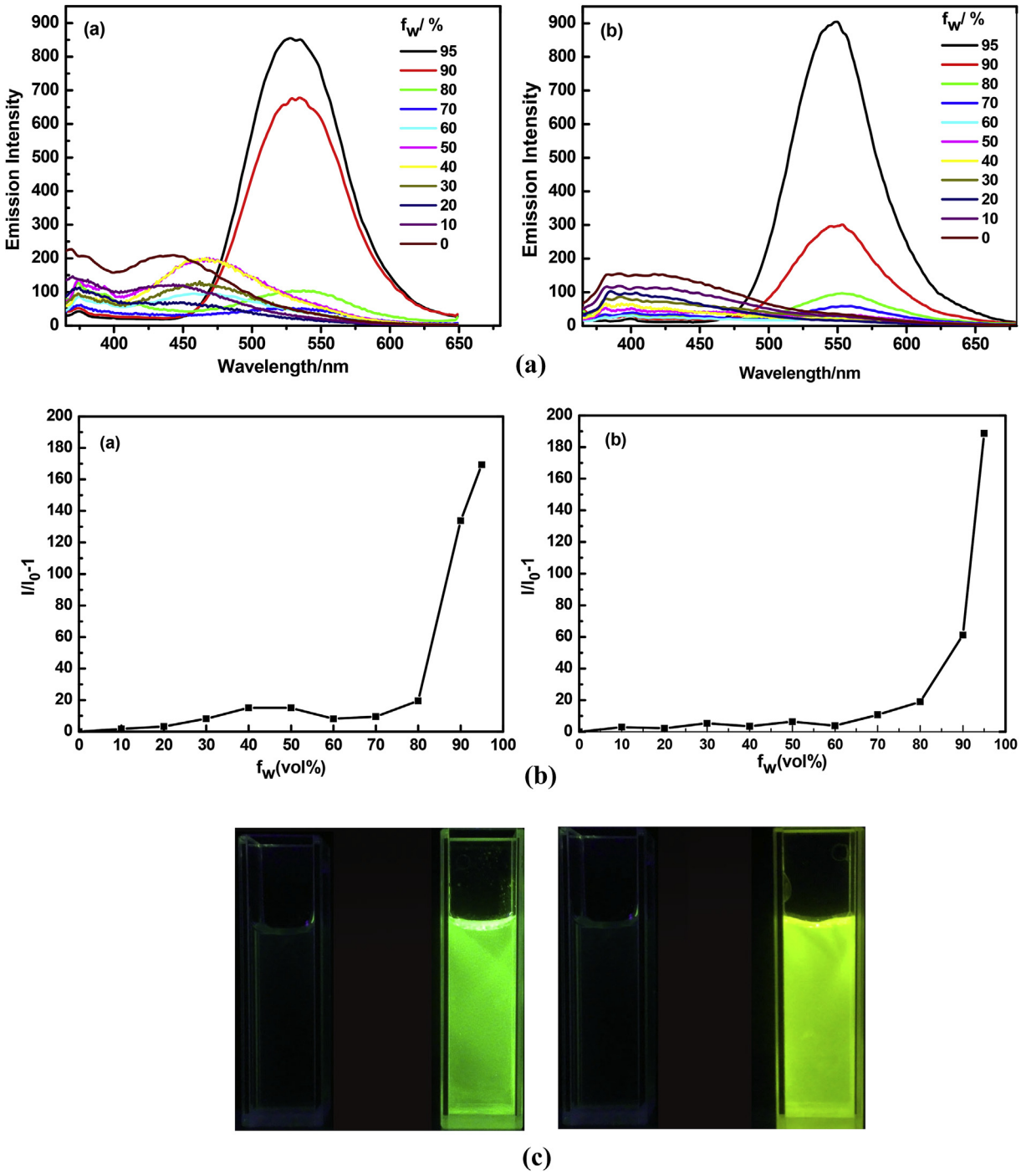

Fig. 1. (a) PL spectra of **PDPBCE** (a) and **BDPBCE** (b) in various water contents of THF-water mixtures (Excited at 330 nm and 350 nm, respectively). (b) Plot of (I/I_o)-1 against water volume fraction (f_w) of **PDPBCE** (a) and **BDPBCE** (b), where I_o and I are the PL intensities without and with water in the THF-water mixtures. (c) Photographic images of **PDPBCE (left)** and **BDPBCE (right)** in THF-water mixture of f_w (i) 0.0 and (ii) 95%.

and **BDPBCE** amount to 3.21 and 3.09 eV, respectively. The results were consistent with the optical band gaps, confirming that the results of DFT calculations obtained using the B3LYP/6-31G(d,p) basis set were in good agreement with the experimental data.

3.6. Electrochemical properties

Cyclic voltammetry (CV) was carried out to investigate the electrochemical properties of **PDPBCE** and **BDPBCE**. All experiments were carried out in acetonitrile containing 0.1 M tetrabutylammonium perchlorate as the supporting electrolyte under a nitrogen atmosphere. The cyclic voltammograms of **PDPBEC** and **BDPBCE** are given in Fig. S6. For **PDPBCE**, the reduction peak at −0.50 V is ascribed to the reduction of the electron-poor dimesitylboron moiety, while the oxidation peak at 1.35 V is assigned to the oxidation of the peripheral carbazole units. **BDPBCE** shows a similar CV to **PDPBCE**, its reversible oxidation and reduction peak are at 1.40 and −0.52 V, respectively. The highest occupied

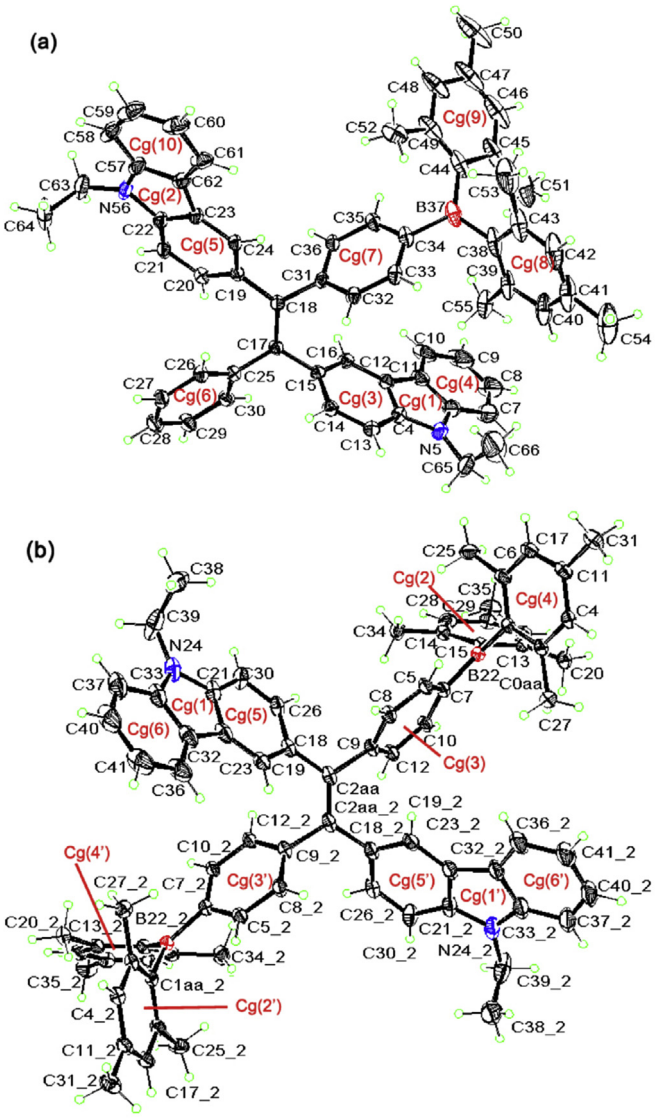

Fig. 2. ORTEP drawings of **PDPBCE** (a) and **BDPBCE** (b) (trans isomer) (CCDC 1414326 and 1417168).

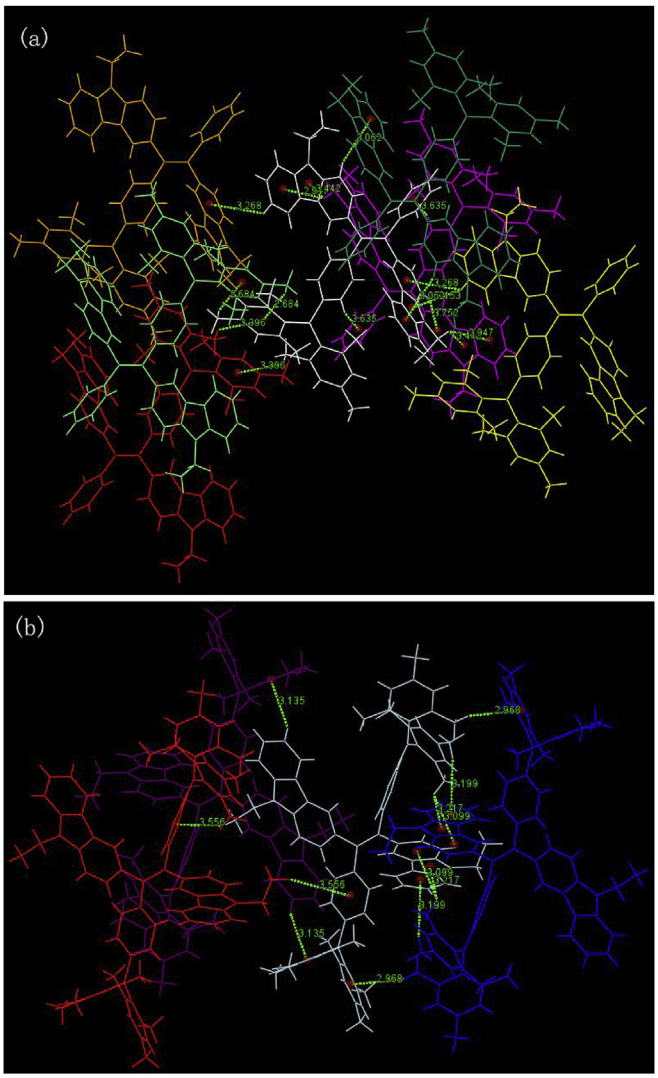

Fig. 3. Crystal packing of **PDPBCE** (a) and **BDPBCE** (b).

molecular orbital (HOMO) energy levels [HOMO = −(4.40 + E_{ox})] were estimated from the onset oxidation potentials, while the lowest unoccupied molecular orbital (LUMO) energy levels [LUMO = −(HOMO + E_g)] were obtained from optical band gaps and HOMO values. The onset oxidation potentials of **PDPBCE** and **BDPBCE** were observed at 0.38 and 0.45 V, respectively. The HOMO energy levels were calculated to be −4.78 and −4.85 eV for **PDPBCE** and **BDPBCE**, respectively. The LUMO energy levels were calculated to be −1.46 and −1.90 eV, respectively. The CV curves remain unchanged under multiple successive potential scans, indicating the excellent redox stability of **PDPBCE** and **BDPBCE**.

3.7. Electroluminescence properties

To evaluate the performance of **PDPBCE** and **BDPBCE** as light-emitting materials in electroluminescent devices, non-doped OLEDs were fabricated and tested in the following architecture: ITO/HATCN (10 nm)/NPB (50 nm)/EML (30 nm)/TPBi (40 nm)/LiF (1 nm)/Al (150 nm) (EML = **PDPBCE** for device A and **BDPBCE** for device B). ITO substrate was used as an anode, dipyrazino[2,3-*f*:2′,3′-*h*]quinoxaline-2,3,6,7,10,11-hexacarbonitrile (HATCN) as a hole-injection layer, *N*,*N*-*bis*(1-naphthyl)-*N*,*N*-diphenylbenzidine (NPB) as a hole-transfer layer, 1,3,5-tris(*N*-phenylbenzimidazol-2-yl)benzene (TPBi) as an electron-transport/hole-block layer, LiF as an electron-injection layer, and Al as a cathode. Fig. S7 presents the EL spectra of device A and device B. The EL spectrum of device A exhibited a maximum emission peak locating at 537 nm, showing that **PDPBCE** emits yellowish-green light with Commission International de L'Eclairage (CIE) coordinates of (0.32, 0.58). The EL spectrum of device B displayed a maximum emission peak at 554 nm with CIE coordinates of (0.38, 0.58), indicating **BDPBCE** emitted greenish-yellow light. The CIE chromaticity coordinates of device A and device B are displayed in Fig. 5. The EL emission of **BDPBCE** is redder than that of **PDPBCE**, which is consistent with the PL observed for the thin films. The EL emissions of device A and device B were slightly red-shifted compared to the thin films and the 95% aqueous solutions, which demonstrate that the EL emissions originate from the amorphous emitting layer. The current density-voltage-luminance curves and the current efficiency-current density curves of device A and device B are depicted in Fig. 6 and Fig. 7, respectively. The electroluminescence data are summarized in Table 3. As shown in Table 3, device A exhibited valuable EL performances with a turn-on voltage of 3.8 V,

Table 2
Analysis of dihedral angles between intramolecular aromatic planes (π rings) and C–H … π intermolecular interactions in the crystal packing of **PDPBCE** and **BDPBCE**.

Com.	Planes (Cg(i), Cg(j))[a]	Angles (°)	Atoms to planes (C(X)-H(xA)/Cg(j))a	Distances (Å)
PDPBCE	Cg(7), Cg(6)	70.48	C(33)-H(33) → Cg(6)	3.635
	Cg(7), Cg(5)	82.60	C(53)-H(53B) → Cg(8)	3.396
	Cg(7), Cg(3)	48.57	C(50)-H(50A) → Cg(9)	2.684
	Cg(7), Cg(9)	64.51	C(65)-H(65B) → Cg(10)	2.947
	Cg(7), Cg(8)	68.54	C(13)-H(13) → Cg(5)	3.752
	Cg(6), Cg(3)	51.47	C(21)-H(21) → Cg(4)	3.062
	Cg(6), Cg(5)	73.09	C(60)-H(60) → Cg(3)	3.628
	Cg(3), Cg(5)	70.14		
BDPBCE	Cg(3), Cg(5)	73.20	C(41)-H(41) → Cg(4)	3.135
	Cg(3), Cg(5′)	66.16	C(38)-H(38A) → Cg(3)	3.556
	Cg(3), Cg(3′)	61.61	C(25)-H(25B) → Cg(4)	2.968
	Cg(3), Cg(4)	81.13	C(34)-H(34A) → Cg(1′)	3.099
	Cg(3), Cg(2)	65.38	C(35)-H(35B) → Cg(6′)	3.199
	Cg(5), Cg(5′)	85.20		

[a] Plane numbers of Cg(i), Cg(j) and atom numbers are from Fig. 2.

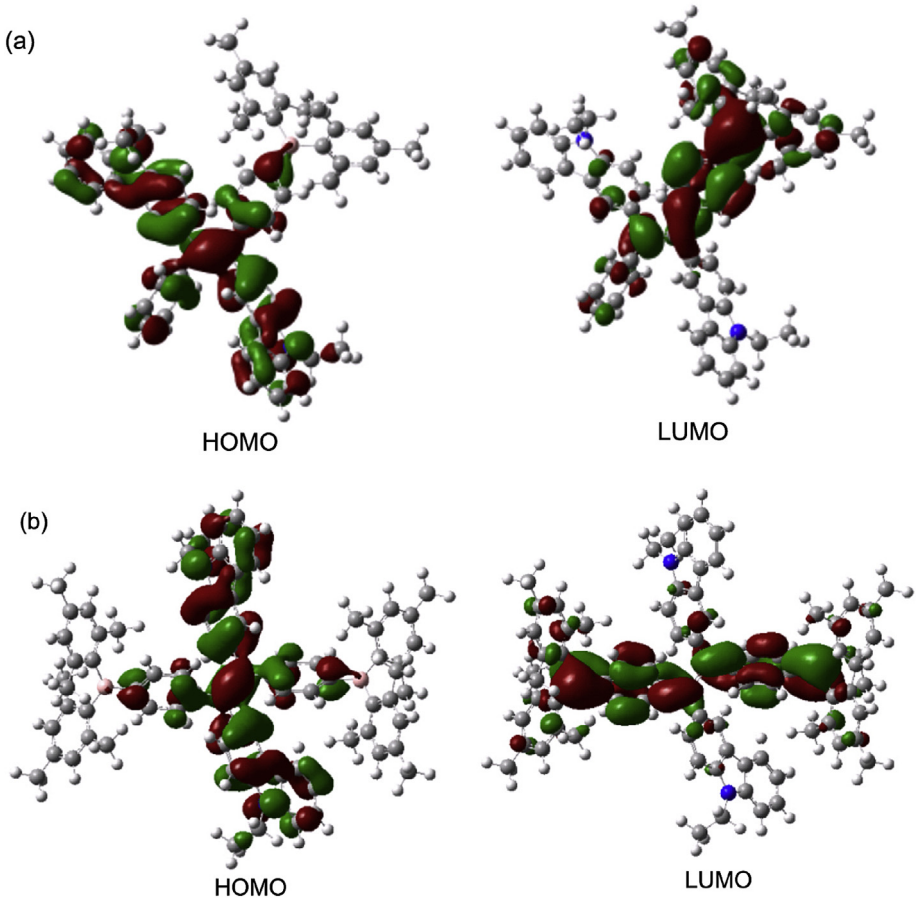

Fig. 4. The HOMO and LUMO distributions of **PDPBCE** (a) and **BDPBCE** (b).

maximum luminous efficiency of 6.4 cd A^{-1} (at 6.8 V) and maximum brightness of 59130 cd m^{-2} (at 15 V). In contrast, device B showed even better EL behavior with a lower turn-on voltage of 3.0 V, higher maximum luminous efficiency and maximum brightness of 11.2 cd A^{-1} (at 5.0 V) and 67500 cd m^{-1} [2] (at 15 V), respectively. Both the devices exhibit very low turn-on voltage and excellent bright luminance, which may due to the high charge-injection rate and the efficient balanced charge-transport properties. The low operation voltage is beneficial for devices to become safer operable and more cost effective due to a lower energy consumption. Such high EL performance indicated the high potential of **PDPBCE** and **BDPBCE** as solid emitters for the construction of efficient EL devices.

4. Conclusions

In this paper, we presented two novel AIE molecules based on carbazole-substituted diphenylethene and dimesitylboron. Their structures were fully characterized by elemental analysis, mass spectrometry, NMR spectroscopy and X-ray diffraction. Due to the existence of the tetraarylethene skeleton, the two compounds exhibited typical AIE-behavior. Both compounds showed high

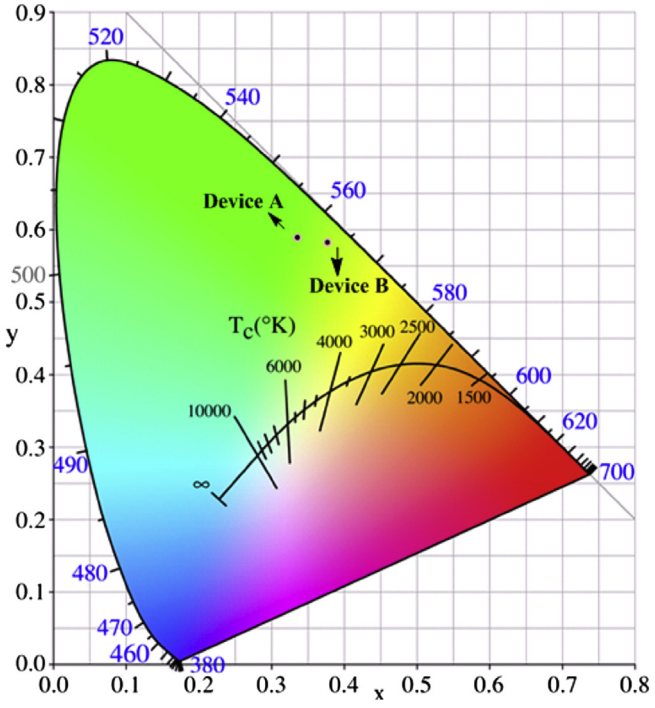

Fig. 5. CIE chromaticity coordinates of **Device A** and **Device B**.

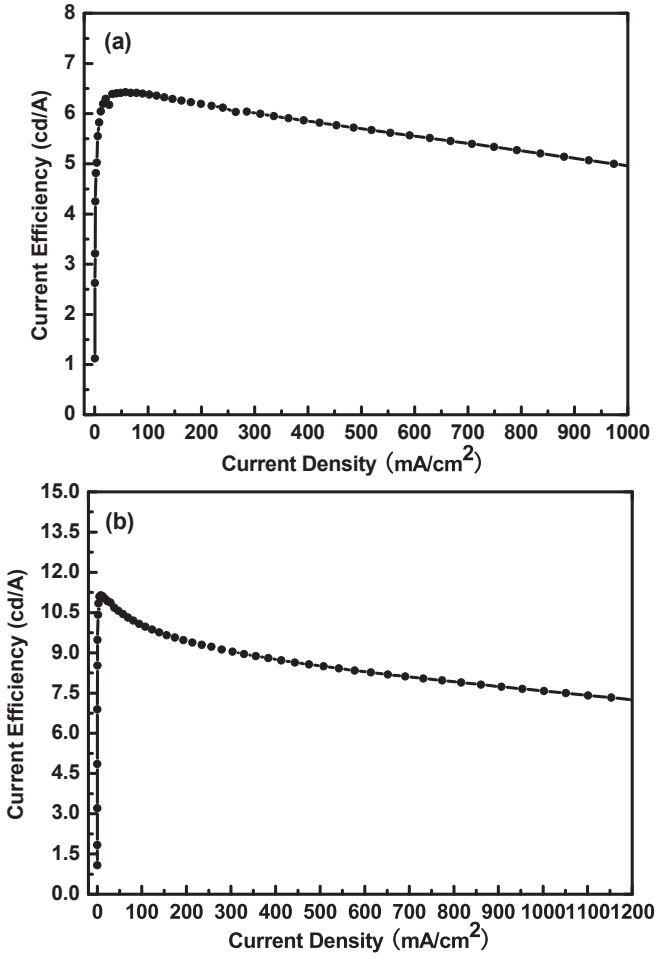

Fig. 6. Current efficiency-current density curves of **Device A** (a) and **Device B** (b).

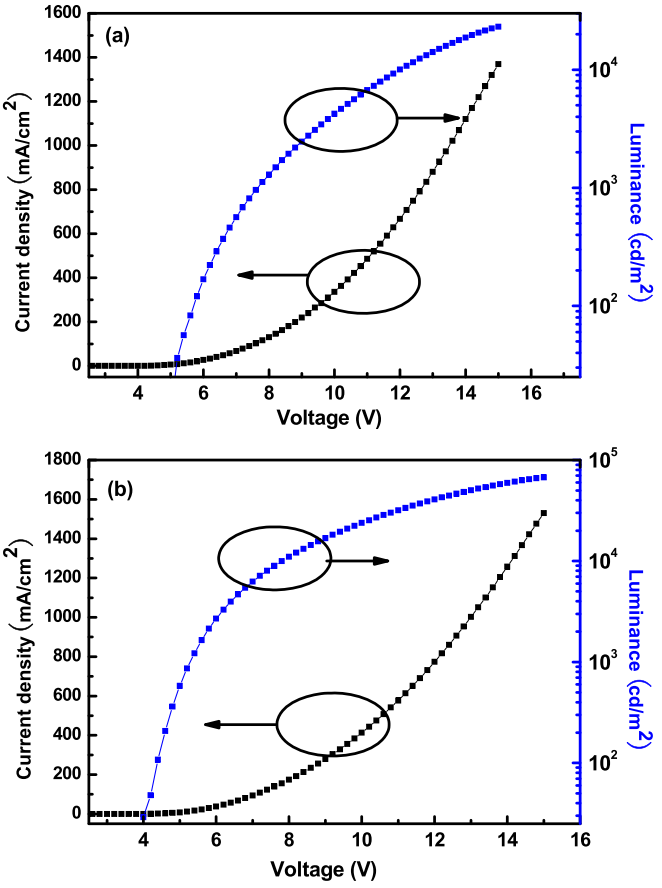

Fig. 7. Current density-voltage-luminance curves of **Device A** (a) and **Device B** (b).

Table 3
Electroluminescent characteristics of **Device A** and **Device B**.

Device	V_{on}[a] (V)	L_{max}[b] (cd/m^2)	CE_{max}[c] (cd/A)	λ_{EL}[d] (nm)	CIE (x, y)
A	3.8	59130 (15 V)	6.43 (6.8 V)	537	(0.34,0.59)
B	3.0	67500 (15 V)	11.2 (5.0 V)	554	(0.39,0.57)

[a] Turn on voltage at a brightness of 1 cd m^{-2}.
[b] Maximum luminance.
[c] Maximum current efficiency.
[d] Electroluminescence peak.

thermal and electrochemical stabilities, which is necessary for fabricating devices with a long lifetime. The photophysical analysis proved that the two luminogens were bright green light emitters, suitable for OLEDs. In order to reveal the AIE mechanism of the two compounds, their single crystal structures including their crystal packing were systematically studied. It turned out that the twisted conformation and multiple intermolecular interactions gave rise to the AIE effect. Finally, the two compounds were utilized as light-emitting layers to fabricate non-doped OLEDs. The results indicated that device A fabricated with **PDPBCE** showed yellowish-green light with a maximum emission peak of 537 nm, a turn-on voltage of 3.8 V, a maximum brightness of 59130 cd m^{-2} and a maximum current efficiency of 6.43 cd A^{-1}; and device B fabricated with **BDPBCE** showed greenish-yellow light with a maximum emission peak of 554 nm, a turn-on voltage of 3.0 V, a maximum brightness of 67500 cd m^{-2} and a maximum current efficiency of 11.2 cd A^{-1}. Thus, we present a versatile strategy to prepare efficient light-emitting materials by introducing of AIE groups into the electron-donor and electron-acceptor system. Extended

investigation and further optimization on the devices based on the donor-acceptor system compounds are being carried out in our laboratory and will be reported in due course.

Acknowledge

This work was supported by Beijing National Laboratory for Molecular Sciences (No. BNLMS 2013031); Science and Technology Innovation Project of Shanxi Province (No. 2014101011); Natural Science Foundation of Shanxi Province (No. 2014011003 and 2015011015); Open Fund of the State Key Laboratory of Luminescent Materials and Devices, South China University of Technology (No. 2014-skllmd-09); Scientific and Technological Innovation Programs of Higher Education Institutions in Shanxi Province (No. 2014109 and 2012005); National Natural Science Foundation of China (No. 61405089); The Innovation of Science and Technology Committee of Shenzhen (No. JCYJ20140417105742713). State Key Laboratory of Structural Chemistry, Fujian Institute of Research on the Structure of Matter, Chinese Academy of Sciences (No. 20140016) and Fund of Key Laboratory of Optoelectronic Materials Chemistry and Physics, Chinese Academy of Sciences (No. 2008DP173016).

Appendix A. Supplementary data

Supplementary data related to this article can be found at http://dx.doi.org/10.1016/j.orgel.2016.03.003.

References

[1] C.W. Tang, S.A. VanSlyke, Appl. Phys. Lett. 51 (1987) 913–915.
[2] J.N. Moorthy, P. Venkatakrishnan, P. Natarajan, D.F. Huang, T.J. Chow, J. Am. Chem. Soc. 130 (2008) 17320–17333.
[3] A.C. Grimsdale, K.L. Chan, R.E. Martin, P.G. Jokisz, A.B. Holmes, Chem. Rev. 109 (2009), 897–1091.
[4] M.T. Lee, C.H. Liao, C.H. Tsai, C.H. Chen, Adv. Mater. 17 (2005) 2493–2497.
[5] P.-Y. Gu, Y. Zhao, J.-H. He, J. Zhang, C. Wang, Q.-F. Xu, J.-M. Lu, X.W. Sun, Q. Zhang, J. Org. Chem. 80 (2015) 3030–3035.
[6] G. Li, Y. Zhao, J. Li, J. Cao, J. Zhu, X.W. Sun, Q. Zhang, J. Org. Chem. 80 (2015) 196–203.
[7] J. Li, Y. Zhao, J. Lu, G. Li, J. Zhang, Y. Zhao, X. Sun, Q. Zhang, J. Org. Chem. 80 (2015) 109–113.
[8] J. Xiao, B. Yang, J.I. Wong, Y. Liu, F. Wei, K.J. Tan, X. Teng, Y. Wu, L. Huang, C. Kloc, F. Boey, J. Ma, H. Zhang, H.Y. Yang, Q. Zhang, Org. Lett. 13 (2011) 3004–3007.
[9] T. Förster, K. Kasper, Z Phys. Chem. 1 (1954) 275–277.
[10] S.W. Thomas III, G.D. Joly, T.M. Swager, Chem. Rev. 107 (2007) 1339–1386.
[11] M. Belletete, J. Bouchard, M. Leclerc, G. Durocher, Macromolecules 38 (2005) 880–887.
[12] K.Y. Pu, B. Liu, Adv. Funct. Mater. 19 (2009) 277–284.
[13] A. Iida, S. Yamaguchi, Chem. Commun. 21 (2009) 3002–3004.
[14] A.C. Grimsdale, K.L. Chan, R.E. Martin, P.G. Jokisz, A.B. Holmes, Chem. Rev. 109 (2009), 897–1091.
[15] A. Menon, M. Galvin, K.A. Walz, L. Rothberg, Synth. Met. 141 (2004) 197–202.
[16] C.-T. Chen, Chem. Mater. 16 (2004) 4389–4400.
[17] J.D. Luo, Z.L. Xie, J.W.Y. Lam, L. Cheng, H.Y. Chen, C.F. Qiu, H.S. Kwok, X.W. Zhan, Y.Q. Liu, D.B. Zhu, B.Z. Tang, Chem. Commun. 18 (2001) 1740–1741.
[18] J. Chen, B. Xu, X.Y. Ouyang, B.Z. Tang, Y. Cao, J. Phys. Chem. A 108 (2004) 7522–7526.
[19] N.L.C. Leung, N. Xie, W. Yuan, Y. Liu, Q. Wu, Q. Peng, Q. Miao, J.W.Y. Lam, B.Z. Tang, Chem. Eur. J. 20 (2014) 15349–15353.
[20] Y. Hong, J.W.Y. Lam, B.Z. Tang, Chem. Soc. Rev. 40 (2011) 5361–5388.
[21] J. Mei, Y. Hong, J.W.Y. Lam, A. Qin, B.Z. Tang, Adv. Mater. 26 (2014) 5429–5459.
[22] H. Wang, E. Zhao, J.W.Y. Lam, B.Z. Tang, Mater. Today 7 (2015) 365–377.
[23] Z.J. Zhao, B.R. He, B.Z. Tang, Chem. Mater. 6 (2015) 5347–5365.
[24] J. Liang, B. Liu, B.Z. Tang, Chem. Soc. Rev. 44 (2015) 2798–2811.
[25] T.K. Kwok, C.W.T. Leung, W.T. Chris, J.W.Y. Lam, B.Z. Tang, Chem. Soc. Rev. 44 (2015) 4228–4238.
[26] G.R. Hu, N.L.C. Lelson, B.Z. Tang, Chem. Soc. Rev. 43 (2014) 4494–4562.
[27] Y.Q. Dong, C.Y. Li, W.J. Zhao, Y.P. Dong, B.Z. Tang, J. Mol. Eng. Mater. 1 (2013) 1340010/1–1340010/13.
[28] D. Ding, K. Li, B. Liu, B.Z. Tang, Acc. Chem. Res. 46 (2013) 2441–2453.
[29] Z.J. Zhao, J.W.Y. Lam, B.Z. Tang, Soft Matter 9 (2013) 4564–4579.
[30] A.J. Qin, J.W.Y. Lam, B.Z. Tang, Prog. Polym. Sci. 37 (2012) 182–209.
[31] Z.J. Zhao, J.W.Y. Lam, B.Z. Tang, J. Mater. Chem. 22 (2012) 23726–23740.
[32] C.Y.K. Chan, Z. Zhao, J.W.Y. Lam, J. Liu, S. Chen, P. Lu, F. Mahtab, X. Chen, H.H.Y. Sung, H.S. Kwok, Y. Ma, I.D. Williams, K.S. Wong, B.Z. Tang, Adv. Funct. Mater. 22 (2012) 378–389.
[33] Z. Zhao, S. Chen, J.W.Y. Lam, P. Lu, Y. Zhong, K.S. Wong, H.S. Kwok, B.Z. Tang, Chem. Commun. 46 (2010) 2221–2223.
[34] B. Xu, Z. Chi, H. Li, Xi Zhang, X. Li, S. Liu, Y. Zhang, J. Xu, J. Phys. Chem. C 115 (2011) 17574–17581.
[35] Z. Zhao, J.W.Y. Lamb, B.Z. Tang, J. Mater. Chem. 22 (2012) 23726–23740.
[36] J. Huang, N. Sun, J. Yang, R. Tang, Q. Li, D. Ma, J. Qin, Z. Li, J. Mater. Chem. 22 (2012) 12001–12007.
[37] V.S. Vyas, R. Rathore, Chem. Commun. 46 (2010) 1065–1067.
[38] W. Wang, T. Lin, M. Wang, T.-X. Liu, L. Ren, D. Chen, S. Huang, J. Phys. Chem. B 114 (2010) 5983–5988.
[39] R. Hu, J.W.Y. Lam, J. Liu, H.H.Y. Sung, I.D. Williams, Z. Yue, K.S. Wong, M.M.F. Yuen, B.Z. Tang, Polym. Chem. 3 (2012) 1481–1489.
[40] O. Paliulis, J. Ostrauskaite, V. Gaidelis, V. Jankauskas, P. Strohriegl, Macromol. Chem. Phys. 204 (2003) 1706–1712.
[41] M. Sonntag, P. Strohriegl, Chem. Mater. 16 (2004) 4736–4742.
[42] K.-T. Wong, Y.-Y. Chien, R.-T. Chen, C.-F. Wang, Y.-T. Lin, H.-H. Chiang, P.-Y. Hsieh, C.-C. Wu, C.H. Chou, Y.O. Su, G.-H. Lee, S.-M. Peng, J. Am. Chem. Soc. 124 (2002) 11576–11577.
[43] J.R. Lakowicz, Principles of Fluorescence Spectroscopy, third ed., Springer, 2006.
[44] I.F. Perepichka, D.F. Perepichka, Handbook of Thiophene-Based Materials: Applications in Organic Electronics and Photonics, John Wiley & Sons, 2009.
[45] Y. Liu, X. Ye, G. Liu, Y. Lv, X. Zhang, S. Chen, J.W.Y. Lam, H.S. Kwok, X. Tao, B.Z. Tang, J. Mater. Chem. C 2 (2014) 1004–1009.
[46] K. Tanaka, Y. Chujo, Macromol. Rapid Commun. 33 (2012) 1235–1255.
[47] F. Cheng, F. Jäkle, Polym. Chem. 2 (2011) 2122–2132.
[48] Z.M. Hudson, S. Wang, Acc. Chem. Res. 42 (2009) 1584–1596.
[49] R. Ziessel, A. Harriman, Chem. Commun. 47 (2011) 611–631.
[50] D. Li, H. Zhang, C. Wang, S. Huang, J. Guo, Y. Wang, J. Mater. Chem. 22 (2012) 4319–4328.
[51] W.Z. Yuan, S. Chen, J.W.Y. Lam, C. Deng, P. Lu, H.H.-Y. Sung, I.D. Williams, H.S. Kwok, Y. Zhang, B.Z. Tang, Chem. Commun. 47 (2011) 11216–11218.
[52] G.-F. Zhang, Z.-Q. Chen, M.P. Aldred, Z. Hu, T. Chen, Z. Huang, X. Meng, M.-Q. Zhu, Chem. Commun. 50 (2014) 12058–12060.
[53] M. Chen, L. Li, H. Nie, J. Tong, L. Yan, B. Xu, J.Z. Sun, W. Tian, Z. Zhao, A. Qin, B.Z. Tang, Chem. Sci. 6 (2015) 1932–1937.